Effect of ridge-ridge interactions in crumpled thin sheets

Shiuan-Fan Liou,[1] Chun-Chao Lo,[1] Ming-Han Chou,[1] Pai-Yi Hsiao,[2] and Tzay-Ming Hong[1,3]
[1]*Department of Physics, National Tsing Hua University, Hsinchu 30013, Taiwan, Republic of China*
[2]*Department of Engineering and System Science, National Tsing Hua University, Hsinchu 30013, Taiwan, Republic of China*
[3]*Center for Fundamental Science Research, National Tsing Hua University, Hsinchu 30013, Taiwan, Republic of China*
(Received 13 May 2013; revised manuscript received 18 October 2013; published 7 February 2014)

We study whether and how the energy scaling based on the single-ridge approximation is revised in an actual crumpled sheet, namely, in the presence of ridge-ridge interactions. Molecular dynamics simulation is employed for this purpose. In order to improve the data quality, modifications are introduced to the common protocol. As crumpling proceeds, we find that the average storing energy changes from being proportional to one-third of the ridge length to a linear relation, while the ratio of bending and stretching energies decreases from 5 to 2. The discrepancy between previous simulations and experiments on the material-dependence for the power-law exponent is resolved. We further determine the average ridge length to scale as $1/D^{1/3}$, the ridge number as $D^{2/3}$, and the average storing energy per unit ridge length as $D^{0.881}$ where D denotes the volume density of the crumpled ball. These results are accompanied by experimental proofs and are consistent with mean-field predictions. Finally, we extend the existent simulations to the high-pressure region and verify the existence of a scaling relation that is more general than the familiar power law at covering the whole density range.

DOI: 10.1103/PhysRevE.89.022404 PACS number(s): 62.20.F−, 46.32.+x, 89.75.Fb

I. INTRODUCTION

Although crumpling is ubiquitous and simple to enact, intense researches to understand its complexities only began in the last thirty years or so. It has not only become relevant to cutting-edge technologies like utilizing crumpled graphene sheets [1] to harvest energies by converting motion into electricity, but is of interest to the general phenomenon of condensation of many outstanding problems in physics [2]. However, some properties of crumpling remain unresolved. For instance, as the developable cones [3–6] increase in number and form the familiar network [7–9] of ridges and vertices, scientists still do not know how they collaborate to produce stunningly simple power laws between the crumpled ball size R and crumpling force F [10–19], $R \sim F^{-\alpha}$, and about the occurring frequency [20–22] of different noise intensities. One challenge is to understand how the crumpled sheet constructs spontaneously a highly porous and yet robust structure [23–25]. Proper theoretical tools are also in demand to tackle the complex many-body interactions among these deformations, especially the self-avoidance that plays an important role [14] at creating the glasslike interior after a series of highly nonequilibrium processes [26], similar to the random packing in a golf ball basket or salt jar.

In view of the theoretic inability, molecular dynamics simulation becomes a powerful tool to obtain information, such as the three-dimensional distribution of ridges and facets before unfolding, the energy storage in each ridge, and how the increase of crumpled ball density affects these quantities. We are interested in the effect of ridge-ridge interactions on the energy scaling predicted by the single-ridge approximation [2,7,9]. Attentions are also paid to resolve major disagreements between previous simulations [14,18] and experiments [16,19]. In the mean time, we push the simulation to a more-time-consuming region of large densities to verify the existence of an alternative scaling law [19]. Finally, we study how the ridge number, average ridge length, and energy cost per unit length evolve with the crumpled ball density, and compare these relations with the mean-field predictions.

II. MOLECULAR DYNAMICS SIMULATION

Our simulations follow a protocol which models a thin sheet by a triangular lattice with bond length $r = 1$ [12,14,18]. Bending and stretching moduli [12], k_B and k_S, are imposed on a two-dimensional circular membrane with radius $R_0 = 130$ lattice sites, which composes of $N_{\text{bead}} = 62\,143$ beads. Simulation on a larger system of $R_0 = 500$ sites, for test, has been checked not to alter our conclusions. The Weeks-Chandler-Andersen (WCA) [27] Lennard-Jones potential is used to ensure that no bead can penetrate each other. Crumpling force is simulated by a collapsing impenetrable spherical wall that encloses the membrane. In order to compare the simulations with the experiments, a realistic value of 1/3 is assigned to the Poisson ratio and the relation $k_B/k_S = 3h^2/32$ is used to constrain k_S with each choice of k_B. The bead diameter is held constant, $h = 0.9$. We also include plasticity by halving the magnitude of k_B beyond a yield angle of 10° and requiring the strain to relax with the original k_B.

III. MECHANICAL RESPONSE OF A SELF-AVOIDING SHEET

We first verify that our simulation reproduces the correct mechanical response. The data plotted in Fig. 1 show how the (dimensionless) density inside the collapsing wall (of radius R_{wall}) $D_1 \equiv N_{\text{bead}}[4\pi(h/2)^3/3]/[4\pi R_{\text{wall}}^3/3]$ varies with the (dimensionless) external pressure $P^\star \equiv (P/Y)(R_0/h)$ where P is the pressure and Y is Young's modulus. The reason why we show D_1 vs $P^\star$ here, instead of R_{wall} vs P (or F), is that this presentation collapses the simulation data of different k_B onto a master curve, irrespective of whether plasticity is included. The results reveal a general scaling relation across

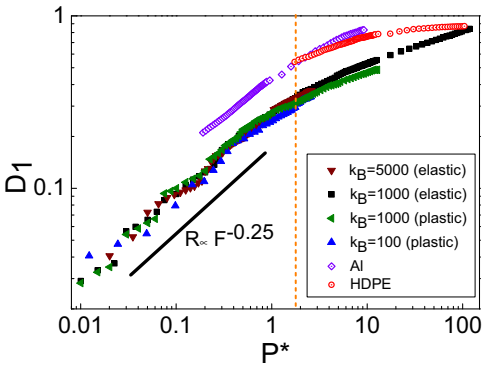

FIG. 1. (Color online) Dimensionless density D_1 vs dimensionless pressure $P^\star$ for elastic and plastoelastic sheets of different k_B by simulations. The ratio of yield stress to Young's modulus for the plastic case is set at 0.175. Experimental data [19] for Al and HDPE are superimposed for comparison. The vertical dashed line roughly marks the region of power-law behavior with the exponent $\alpha = 0.25 \pm 0.01$.

the whole range of P, which can be reduced to a power law $D_1 \sim P^{\star 3\alpha/(1+2\alpha)}$ at small densitities. We find that the exponent α is 0.25, in good agreement with simulations obtained by other groups [14,18]. However, a discrepancy is observed when we superimpose experimental data [19] on the same figure for comparison where the density $\pi R_0^2 h/[4\pi R^3/3]$ is calculated from the empirically observed radius R of the crumpled ball. The densities for aluminum foils (Al) and high-density polyethylene (PE) film (HDPE) are significantly larger than the simulation ones.

The first reason that leads to the discrepancy is the coarse-grained triangular model used here. The numerator of D_1 uses the total volume of beads on the simulating sheet, $V_{\text{beads}} \equiv N_{\text{bead}}[4\pi(h/2)^3/3]$, but actual samples like Al or HDPE have no meshes. So V_{beads} should be replaced by $V_{\text{sheet}} \equiv \pi R_0^2 h$. Secondly, the volume V of the crumpled ball (of beaded net) is overestimated by $V_{\text{wall}} = 4\pi R_{\text{wall}}^3/3$ in the denominator of D_1. By the time the radius-force power law sets in, the inside and outside of a crumpled ball can roughly be defined. Similar to eggs in an egg carton, there are voids between the crumpled ball and the confining wall, as demonstrated by Fig. 2(b). Their volume difference $\Delta V_{\text{void}} = V_{\text{wall}} - V$ constitutes another source of error to D_1. Finally, since the power law is expected to be strictly valid only in the limit of $V \gg V_{\text{sheet}}$, it is natural to expect artifacts when V becomes small. A serious example is the growing number of beads that become wedged in the mesh of the triangular lattice, as sketched in Fig. 2(a). Since a real paper sheet can not cut into itself, we compensate for the crumpled ball volume V by allowing it to swell by the same amount of volume ΔV_{wedged} wedged inside all gray prisms in Fig. 2(a). Compared to V which denotes the volume of a crumpled ball of beaded net, $V + \Delta V_{\text{wedged}}$ represents more correctly the volume of a crumpled ball of unbroken sheet. To avoid confusion, please consult Table I for the definitions of the different volume and density parameters used in our simulation.

In summary, a more precise definition for the dimensionless density should be $D_2 = (\pi R_0^2 h)/(V + \Delta V_{\text{wedged}})$ where

TABLE I. Definitions of the different volume and density parameters used in our simulation.

Notation	Definition	Description
V_{beads}	$N_{\text{bead}}[4\pi(h/2)^3/3]$	Volume of beaded net
V_{sheet}	$\pi R_0^2 h$	Volume of unbroken sheet
V_{wall}	$4\pi R_{\text{wall}}^3/3$	Volume of confining wall
V		Volume of crumpled ball of beaded net
	$V + \Delta V_{\text{wedged}}$	Volume of crumpled ball of unbroken sheet
ΔV_{wedged}	Fig. 2(a)	Wedged volume inside all gray prisms
ΔV_{void}	$V_{\text{wall}} - V$	Volume of void between confining wall and outer surface of crumpled ball
D_1	$V_{\text{beads}}/V_{\text{wall}}$	Poor definition of crumpled ball density
D_2	$V_{\text{sheet}}/(V + \Delta V_{\text{wedged}})$	Better definition of crumpled ball density

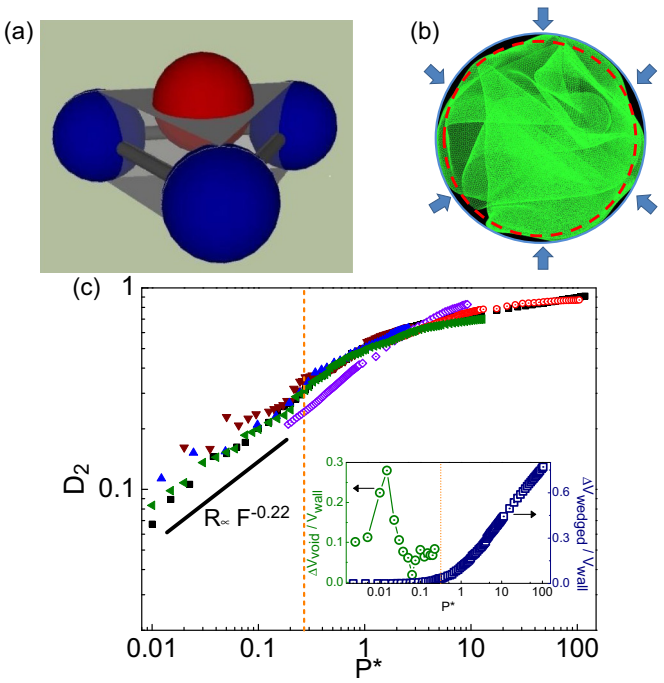

FIG. 2. (Color online) (a) Schematic plot for a (red) bead partially wedged in the interior (the gray prism) of a triangular lattice of (blue) beads. (b) The crumpled ball occupies a volume which, if transformed into a sphere, is marked by the red dashed line with a radius smaller than R_{wall}. The space between the collapsing wall and outer surface of the ball is painted in black and denoted by ΔV_{void}. (c) Dimensionless density D_2 vs dimensionless pressure $P^\star$. Data are replotted from Fig. 1. The power-law region shrinks from $P^\star \leqslant 1.8$ to 0.28, and α decreases from 0.25 to about 0.22 ± 0.02. The inset shows that $\Delta V_{\text{void}}/V_{\text{wall}}$ and $\Delta V_{\text{wedged}}/V_{\text{wall}}$ dominate the small and large pressure regions, respectively, for the case of a $k_B = 1000$ elastic sheet.

$V = V_{\text{wall}} - \Delta V_{\text{void}}$. Figure 2(c) shows D_2 vs $P^\star$ for the different sets of simulation data together with the experimental ones, where the ratios for the volume differences, $\Delta V_{\text{void}}/V_{\text{wall}}$ and $\Delta V_{\text{wedged}}/V_{\text{wall}}$, are also shown in the inset for illustration. We observe that the sets of simulation data are now collapsed with the experimental ones, while retaining the scaling relation. In the mean time, the power-law region shrinks and the exponent reduces to around 0.22. The latter is not hard to understand because $\Delta V_{\text{void}}/V_{\text{wall}}$ in the inset of Fig. 2(c) dominates at small densities and raises D_1, while $\Delta V_{\text{wedged}}/V_{\text{wall}}$ rules at large densities to reduce D_1. Both effects combine to level off the line that represents the power law in Fig. 1. As for the shortening of the already narrow pressure range, it may highlight the possibility that crumpling just does not scale as a power law.

Please notice that experimentalists usually focus on the response in a relatively large density region where the power-law relation is not so well-established, as shown in Fig. 2 for Al and HDPE. It explains why α obtained from experiments [16,19] is usually smaller and nonuniversal. This is because there exists a lower limit to apply external pressure P in crumpling experiments [16,19] where high-pressure nitrogen gas was used to provide the ambient pressure. Since the pressure is balanced, the sheet needs to be precrumpled and packed by a polyvinylchloride (PVC) wrap with the wrap interior maintained at atmospheric pressure via a PE tube connecting to the outside of the pressure chamber. This procedure sets a lower value to P and, therefore, it is not easy for experimentalists to investigate crumpling in the low-pressure region.

IV. ENERGY SCALING BEYOND THE SINGLE-RIDGE APPROXIMATION

It is known that the single-ridge approximation [2,7,9] predicts a scaling law for the energy E to create a folding ridge on a sheet as a one-third power of the ridge length ℓ. If E is partitioned into the bending energy E_B and the stretching energy E_S, the ratio of the two energies is shown to be $E_B/E_S = 5$. Although the former prediction has been checked by simulations for a solitary ridge [18], the two predictions have not yet been verified in a realistic case of crumpling where multiple ridges are formed and interact between each other. Since the ridges are not formed in an equilibrium state, a full relaxation of stress is not expected, particularly when the sheet is crumpled into a very tight space.

We apply a watershed algorithm to determine the folding ridges of the sheet. The data are improved manually by connecting broken segments of the ridges obtained [see Figs. 3(a) and 3(b) for example]. We observe that the distribution of ridge lengths follows a log-normal distribution as shown in Fig. 3, which agrees with theoretical predictions [2,7], experiments [28,29], and other simulations [14]. Moreover, we calculate the energy associated with each ridge generated. The mean energy $E(\ell)$ exhibits a power-law dependence ℓ^γ on the ridge length ℓ, as shown in Fig. 4(a). The exponent γ is then plotted in Fig. 4(b) as a function of inverse density D_2. We find that the predicted value $1/3$ of Witten's single-ridge approximation is recovered in our simulations at low densities. As the density increases, γ rises and saturates asymptotically to 1. In the mean

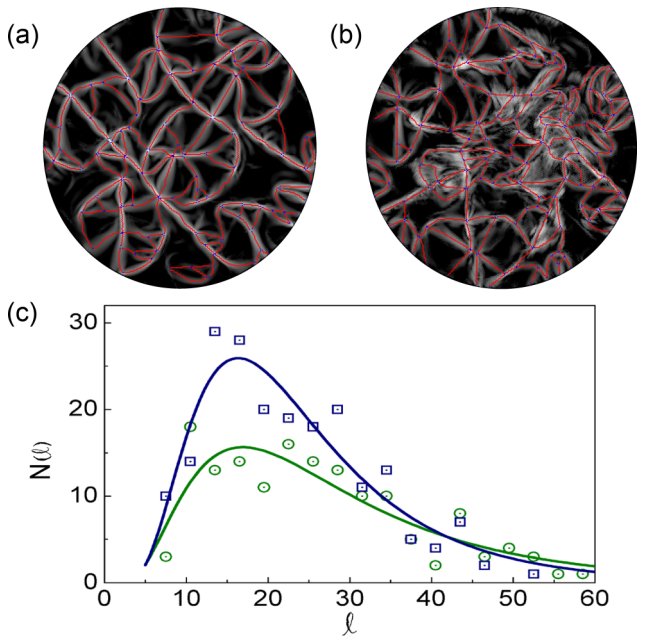

FIG. 3. (Color online) (a) Network of ridges on a crumpled elastic net of beads with $k_B = 1000$ at $D_2 = 0.339$. (b) Same as (a) but on a plastic net. (c) $N(\ell)$ as a function of ℓ. The distribution is fitted by $N(\ell) = A/(\ell B)\exp\{-[\ln(\ell/\ell_0)/B]^2\}$ with $(A,B,\ell_0) = (279,0.87,24.7)$ for an elastic net (circles) and $(364,0.75,21.6)$ for a plastic net (squares).

while, the ratio E_B/E_S drops from the single-ridge value 5 to about 2 [see Fig. 4(c)]. Therefore, the weight of energy gradually shifts from E_B to E_S as D_2 increases, whereas both energies are promoted by the ridge-ridge interactions. Since the dependence of E_B/E_S on D_2 cannot be predicted by the single-ridge approximation, our results show that the ridge-ridge interactions play an important role on the energy storage of sheet.

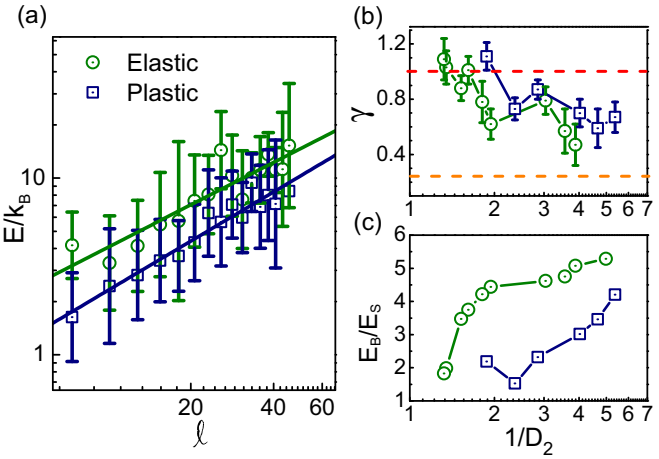

FIG. 4. (Color online) (a) Average storing energy $E(\ell)$ in a ridge as a function of ℓ at $D_2 = 0.339$ and $k_B = 1000$. Least square fits yield $\gamma = 0.813 \pm 0.100$ and 0.943 ± 0.069 for the elastic and plastic sheets, respectively. (b) γ vs $1/D_2$. (c) E_B/E_S vs $1/D_2$.

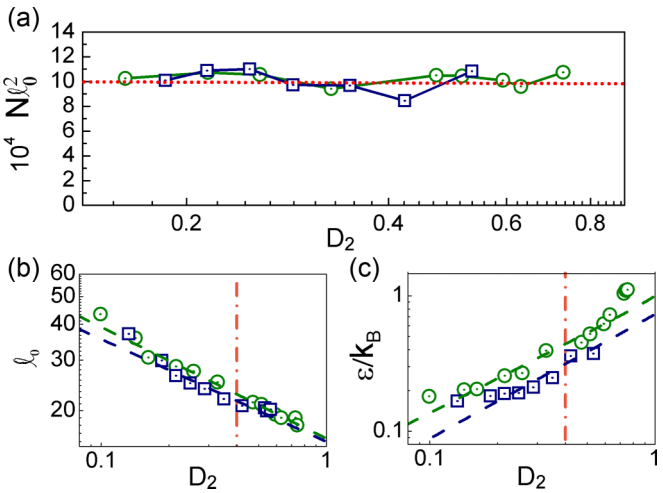

FIG. 5. (Color online) (a)$N\ell_0^2$ vs D_2 for thin sheets with $k_B = 1000$. (b) ℓ_0 vs D_2. The straight-line fitting gives power-law exponents of -0.389 ± 0.048 and -0.358 ± 0.037, respectively, for elastic (circles) and plastic (squares) sheets. (c) Power law dependence of ε on D_2 with exponents 0.846 ± 0.147 and 0.916 ± 0.180, respectively. The first data point at low confinement is not included in the fitting because the radius-force power law has not yet set in. The red dashed-dotted lines in (b) and (c) mark the region of the power-law behavior in Fig. 2.

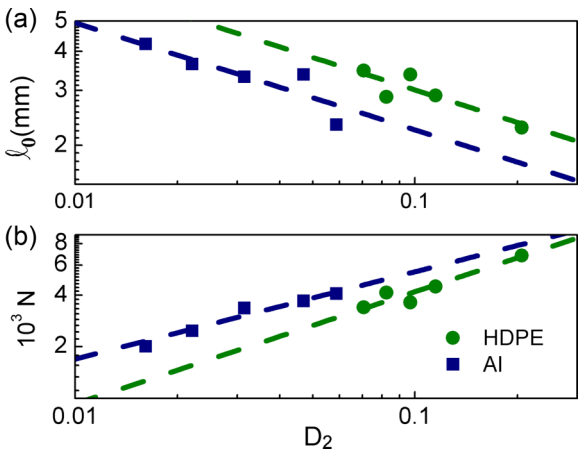

FIG. 6. (Color online) (a) ℓ_0 vs D_2 reveals a power-law relation with exponents -0.342 ± 0.100 for HDPE and -0.346 ± 0.130 for Al. (b) N vs D_2 gives exponents of 0.656 ± 0.09 for HDPE and 0.510 ± 0.07 for Al.

V. RIDGE LENGTH, RIDGE NUMBER, AND THE MEAN-FIELD APPROXIMATION

Having seen how the ridge-ridge interactions complicate and revise the energy scaling, we now study some other properties that turn out to obey the prediction of a simple mean-field theory. As shown in Fig. 5(a), the ridge number N multiplied by the square of the mean ridge length ℓ_0 is essentially constant over the whole range of density D_2. Suppose that the ridges are arranged in a square lattice, then the area of this checkerboard approximately equals $N\ell_0^2/2$, which is consistent with the sheet area $\pi R_0^2 = 5.3 \times 10^4$. Thus, the fact that $N\ell_0^2$ does not change with D_2 can be explained within a mean-field picture. Figure 5(b) shows that $\ell_0 \sim 1/D_2^{1/3}$, which implies that the variation of ℓ_0 is mainly influenced by the geometric confinement, although its magnitude depends on the rigidness of a sheet. This conjecture is compatible with the observation that the power-law behavior in Fig. 5(b) enters at an earlier stage than Fig. 5(c) which involves the mechanical response and energy consideration. Figures 5(a) and 5(b) together say that $N \sim D_2^{2/3}$. Notice that these results are consistent with the experimental findings of $N \sim D^{0.5}$ and $\ell_0 \sim 1/D^{0.27}$ in paper [30], but at odds with the prediction $N \sim D^{4/3}$ and $\ell_0 \sim 1/D^{0.55}$ by previous simulations [14,18] for self-avoiding sheets. It is worth mentioning that the original power laws for N, ℓ_0, and the average energy per unit ridge length ϵ were discovered as a function of pressure which spans more orders of magnitude than the density. The reason why we decided to convert their dependence to D_2 by use of the power law in Fig. 2 is that this makes Fig. 5 more insightful.

Figure 5(c) shows that the average energy per unit ridge length is not merely a material property, but increases with density as $\varepsilon \sim D_2^{\eta}$ where $\eta \sim 0.916$ for elastic and 0.846 for plastic sheets in the power-law region. It implies that the total energy stored in the ridges, $N\ell_0\varepsilon$, scales roughly as $D_2^{1.214}$. In the mean time, the total work W done on the crumpling force can be estimated by $\int_{R_0}^{R} F \cdot dR'$, which yields $R^{(-1/\alpha)+1}$. Adopting the value $\alpha \approx 0.22$ obtained in Fig. 2(c), the scaling of energy input $W \sim D_2^{1.182}$ is consistent with that of energy storage $N\ell_0\varepsilon$.

Regarding the discrepancy between Figs. 5(a), 5(b) and previous simulations [14,18], we decide to resort to more experimental proofs. Our sample preparation and crumpling procedures have been described in Ref. [19]. The high-pressure chamber provides a better-controlled ambient pressure for the three-dimensional crumpling than hand-crushing [30]. The coordinate measuring machine is employed to measure the sample topography, and an image process aided by the calculation of the ridge response function is developed [31] to detect the ridges automatically. Instead of linking the vertices by straight lines [29], we achieve a better resolution that retains the curvy nature of ridges. As shown in Fig. 6, the experimental results are consistent with those of Ref. [30] and in support of Figs. 5(a) and 5(b).

VI. CONCLUSIONS

In conclusion, molecular dynamics simulation has been employed to study the effect of ridge-ridge interactions on a crumpling of self-avoiding sheet. Energy scaling based on the single-ridge approximation is valid only at low densities. Revision is needed as the ridge-ridge interaction intensifies in the high-density region. We manage to conciliate the different exponents α between simulations and experiments. We investigate how the average ridge number, the average ridge length, and the average storing energy per unit length vary with the ball density. The relations are accompanied by experimental proofs and found to be consistent with the mean-field predictions. In the mean time, we extend our simulations to pressure beyond the validity of the power law and confirm the existence of a more general scaling relation.

ACKNOWLEDGMENTS

We thank Professor Kuo-Ning Chiang for the access to a coordinate measuring machine, Professor Chiou-Ting Hsu and M. Huang for the assistance in the image process, and Neil Yenchih Lin for helpful discussions. Hospitalities from the Physics Division of National Center for Theoretical Sciences in Hsinchu and support by the National Science Council in Taiwan are also gratefully acknowledged.

[1] J. Zang, S. Ryu, N. Pugno, Q. Wang, Q. Tu, M. J. Buehler, and X. Zhao, Nat. Mater. **12**, 321 (2013).
[2] A. J. Wood, Physica A **313**, 83 (2002).
[3] S. Chaïeb, F. Melo, and J. C. Géminard, Phys. Rev. Lett. **80**, 2354 (1998).
[4] E. Cerda and L. Mahadevan, Phys. Rev. Lett. **80**, 2358 (1998).
[5] E. Cerda, S. Chaïeb, F. Melo, and L. Mahadevan, Nature (London) **401**, 46 (1999).
[6] J. W. Wang and T. A. Witten, Phys. Rev. E **80**, 046610 (2009).
[7] A. Lobkovsky, S. Gentges, H. Li, D. More, and T. A. Witten, Science **270**, 1482 (1995).
[8] A. E. Lobkovsky and T. A. Witten, Phys. Rev. E **55**, 1577 (1997).
[9] T. A. Witten, Rev. Mod. Phys. **79**, 643 (2007).
[10] Y. Kantor, M. Kardar, and D. R. Nelson, Phys. Rev. Lett. **57**, 791 (1986).
[11] Y. Kantor and D. R. Nelson, Phys. Rev. Lett. **58**, 2774 (1987).
[12] H. S. Seung and D. R. Nelson, Phys. Rev. A **38**, 1005 (1988).
[13] K. Matan, R. B. Williams, T. A. Witten, and S. R. Nagel, Phys. Rev. Lett. **88**, 076101 (2002).
[14] G. A. Vliegenthaqrt and G. Gompper, Nat. Mater. **5**, 216 (2006).
[15] A. S. Balankin, I. C. Silva, O. A. Martinez, and O. S. Huerta, Phys. Rev. E **75**, 051117 (2007).
[16] Y. C. Lin, Y. L. Wang, Y. Liu, and T. M. Hong, Phys. Rev. Lett. **101**, 125504 (2008).
[17] T. Tallinen, J. A. Åström, and J. Timonen, Phys. Rev. Lett. **101**, 106101 (2008).
[18] T. Tallinen, J. A. Åström, and J. Timonen, Nat. Mater. **8**, 25 (2009).
[19] W. Bai, Y. C. Lin, T. K. Hou, and T. M. Hong, Phys. Rev. E **82**, 066112 (2010).
[20] E. M. Kramer and A. E. Lobkovsky, Phys. Rev. E **53**, 1465 (1996).
[21] P. A. Houle and J. P. Sethna, Phys. Rev. E **54**, 278 (1996).
[22] J. P. Sethna, K. A. Dahmen, and C. R. Myers, Nature (London) **410**, 242 (2001).
[23] A. D. Cambou and N. Menon, Proc. Natl. Acad. Sci. USA **108**, 14741 (2011).
[24] Y. C. Lin, J. M. Sun, H. W. Yang, Y. K. Hwu, C. L. Wang, and T. M. Hong, Phys. Rev. E **80**, 066114 (2009).
[25] Y.-C. Lin, J.-M. Sun, J.-H. Hsiao, Y. K. Hwu, C. L. Wang, and T.-M. Hong, Phys. Rev. Lett. **103**, 263902 (2009).
[26] H. Aharoni and E. Sharon, Nat. Mater. **9**, 993 (2010).
[27] J. D. Weeks, D. Chandler, and H. C. Andersen, J. Chem. Phys. **54**, 5237 (1971).
[28] D. L. Blair and A. Kudrolli, Phys. Rev. Lett. **94**, 166107 (2005).
[29] C. A. Andresen, A. Hansen, and J. Schmittbuhl, Phys. Rev. E **76**, 026108 (2007).
[30] A. S. Balankin, A. Horta Rangel, G. Garcia Perez, F. Gayosso Martinez, H. Sanchez Chavez, and C. L. Martinez-Gonzalez, Phys. Rev. E **87**, 052806 (2013).
[31] M. Huang, C. T. Hsu, and K. Tanaka, IEEE Trans. Image Process **21**, 4498 (2012).